

## Electronic relaxation effects on x-ray spectra of titanium and transition-metal carbides and nitrides

A. Balzarotti

*Istituto di Fisica "G. Marconi," Università di Roma, Roma, Italy  
and Gruppo "Programma Utilizzazione della Luce di Sincrotrone," Laboratori Nazionali di Frascati, Frascati, Italy*

M. De Crescenzi

*Dipartimento di Fisica, Università della Calabria, Arcavacata di Rende, Cosenza, Italy  
and Gruppo "Programma Utilizzazione della Luce di Sincrotrone," Laboratori Nazionali di Frascati, Frascati, Italy*

L. Incoccia

*Gruppo "Programma Utilizzazione della Luce di Sincrotrone," Laboratori Nazionali di Frascati, Frascati, Italy*

(Received 7 August 1981)

High-resolution titanium  $K$  x-ray absorption spectra from pure metal, carbide, and nitride are measured using synchrotron radiation. It is shown that the local partial density of states at the metal site is adequate to describe the near-edge features observed. The magnitude of the electron screening to a suddenly switched-on core-hole potential is investigated and found to be correlated to the density of occupied electron states at the Fermi surface. The dynamical aspects of the screening process show up in the extended x-ray absorption fine-structure region of the spectra and influence the phase and amplitude of the photoelectron wave function. Several structural properties of these compounds are also considered.

### I. INTRODUCTION

Metallic carbides and nitrides belong to a class of refractory transition-metal compounds which exhibit a number of unique physical properties such as high melting temperatures and great hardness, which are typical of covalent crystals, as well as good metallic conductivity.<sup>1</sup> They crystallize in a face-centered-cubic rocksalt structure in which metalloid atoms occupy the octahedral interstices of the close-packed sublattice of metallic atoms. Departure from stoichiometry is commonly found<sup>2</sup> due mainly to the carbon lattice vacancies in carbides<sup>3</sup> and/or metal vacancies in nitrides.<sup>4</sup> Since these materials combine properties of insulators and metals, they are not only interesting for technological applications but also from a fundamental point of view. The direction and the amount of charge transfer between the metal and nonmetal atoms, which is connected to the ionic character of their bond, have been the subject of long debate,

and several theoretical studies for TiC (Refs. 5–11) and TiN (Ref. 11) which favor either model have been reported. The largest differences between the methods employed—augmented plane wave (APW) and semiempirical tight-binding—were in the density of states (DOS) and the direction of the charge transfer. This controversy has now been resolved experimentally. Experimental data—x-ray emission<sup>12–15</sup> and absorption,<sup>15</sup> soft x-ray,<sup>10,16,17</sup> and ultraviolet<sup>18–20</sup> photoemission measurements—support strongly the electron transfer of charge from titanium to metalloid. Moreover, the valence and conduction states near the Fermi level ( $E_F$ ) are fairly well probed by photoemission<sup>19–21</sup> and optical<sup>22–24</sup> measurements, but the detailed structure of the energy bands up to 20 eV above  $E_F$  has not conclusively been established so far. We have recently found that valuable information on the Ti  $3d$ -like final states may be provided by high-resolution near-edge spectra of titanium perovskites.<sup>25</sup>

In this paper we present an analysis of the electronic excitations of titanium metal and stoichiometric titanium carbide and nitride based on measurements of x-ray absorption spectra above the Ti  $K$ -threshold using synchrotron radiation. We will show that the one-electron treatment based on the local partial DOS and transition probability concepts describes fairly well the details of near-edge structures but dynamical relaxation effects have to be considered in the extended x-ray absorption fine-structure (EXAFS) regime. More specifically, from the comparison between x-ray  $L$  absorption (XAS), emission (XES), and x-ray photoemission (XPS) data, we find that the magnitude of screening of a suddenly created core hole, determined by the redistribution of charge in the final state, depends on the density of occupied states at the Fermi level. In metallic titanium the flow of charge leads to complete screening, and all spectral edges coincide with the Fermi level. In the carbides and nitrides the screening is less complete than in the metal, because of the lower movable charge density at  $E_F$ , and the XPS edges do not coincide with the XAS and XES edges. In all cases, however,  $E_F$  should be placed at the emission threshold which corresponds to a fully relaxed ion core. At energies of interest for EXAFS (100–1000 eV beyond threshold) the time dependence of the central atom potential is expected to modify the amplitude and phase of the excited photoelectron in a way which depends upon the kinetic energy of the photoelectron. Such modifications are genuine many-body corrections to the one-electron EXAFS theory which involve an energy-dependent reduction factor  $S_0^2$  for the EXAFS amplitude, as discussed by Stern *et al.*<sup>26</sup> The corrections to the total backscattering phase  $\phi(k)$  of the photoelectron are also important and we concentrate mainly on this aspect in the discussion of the EXAFS spectra of titanium carbide and nitride. In these metals we find that the unscreened potential used by Lee and Beni<sup>27</sup> to calculate the central atom phase shift  $2\delta(k)$  is too large for low-energy photoelectrons when the core hole is screened by the conduction electron gas. Similar conclusions seem to hold for bromine molecules<sup>28</sup> and aluminum.<sup>29</sup> From the theoretical side, the effects of dynamical screening on the central atom potential have been recently considered by Noguera and Spanjaard, who present quantitative estimations for aluminum.<sup>30</sup>

Finally, we examine the reliability of phase shifts for the light elements C and N and we con-

clude that the use of the theoretical phase and amplitude functions of Teo and Lee<sup>31</sup> for low- $Z$  atoms gives only qualitative agreement with the experiment.

In Sec. II we outline some experimental details. In Sec. III A we analyze the near  $K$ -edge regions of Ti, TiC and TiN within the one-electron scheme, while in Sec. III B we consider the effects of the electron-electron interactions. Section IV deals with the analysis of the EXAFS part of the spectra.

## II. EXPERIMENTAL

The experiments were performed at the x-ray beam line of the Frascati synchrotron radiation facility PULS (Programma Utilizzazione della Luce di Sincrotrone). The storage ring ADONE was operated at an energy of 1.5 GeV, and the typical electron current was 50 mA.

The radiation was monochromatized by a channel-cut Si(220) crystal and monitored by a gas ionization chamber  $I_0$ . The experimental apparatus used to perform x-ray absorption measurements has been described elsewhere.<sup>32</sup> We reproduce in Fig. 1 the measured intensity versus the photon energy of the light emerging from the monochromator under the conditions specified in the figure. In the spectral range of interest for this

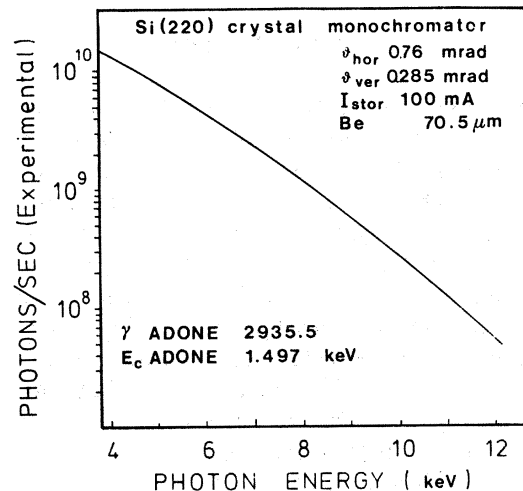


FIG. 1. Photon flux measured at the exit of the Si(220) channel-cut monochromator. The source of radiation is the storage ring ADONE.  $\gamma$  represents the electron energy in units of electron rest energy  $m_0c^2$  and  $E_c$  is the critical energy.  $\vartheta_{\text{hor}}$  and  $\vartheta_{\text{vert}}$  are the horizontal and vertical angles with respect to the electron orbit plane seen by the detector.  $I_{\text{stor}}$  is the average current in the machine.

work, the vertical divergence of the source is about 0.12 mrad. This implies an average resolution  $\Delta E/E \approx 10^{-4}$ , using a 1-mm entrance slit before the monochromator.

The spectral purity of the light, determined by a Si(Li) detector,<sup>32</sup> was fairly good, containing less than 1.4% of second harmonic and 0.01% of third harmonic at 5 keV. The intensity transmitted through the sample was collected by a second chamber  $I_1$ . Both chambers were filled with Ar gas at a pressure chosen to provide a 20% absorption for  $I_0$  and maximum absorption for  $I_1$ . Two slits, of dimensions smaller than the sample, were placed at the entrance and at the exit of the sample vacuum chamber and carefully aligned in order to minimize spurious effects. During a typical scan of the monochromator from 5 to 6 keV the beam spanned a distance of about 4 mm on the vertical plane, and the sample holder moved accordingly to follow the beam, within an accuracy of 100  $\mu\text{m}$ .

A PDP 11/03 computer controlled the whole apparatus and the data collection.<sup>33</sup> The carbides and nitrides were 99.9% pure polycrystalline powders obtained from the Material Research Corp., N.Y. They were stoichiometric  $\text{TiC}_{1.00}$  and  $\text{TiN}_{1.00}$  samples chemically refined and vacuum melted with an oxygen content less than a few ppm. For the measurements the samples were prepared in form of powders sandwiched between two stripes of kapton tape. The Ti samples were 6- $\mu\text{m}$ -thick films free of pinholes. Great care was taken to ensure uniformity over the samples area exposed to the beam. All spectra were measured at room temperature.

### III. RESULTS AND DISCUSSION

#### A. X-ray absorption near-edge structure

Figure 2 shows the x-ray absorption near-edge structure of Ti, TiC, and TiN in the region of the Ti  $K$ -shell excitation. The absorption coefficient starts rising around 4964 eV, which corresponds to the excitation of electrons to the Fermi level, and in titanium compounds it remains low over a region of few eV before rising again rather steeply. The region of relatively weak absorption is quite characteristic of the lowest conduction band DOS of Ti compounds, as found in  $\text{TiO}_2$  and perovskites<sup>25</sup> and, more recently, in some transition-metal dichalcogenides.<sup>34</sup> In all these compounds, the lowest conduction band is formed by the degenerate metal  $3d$  states split by the octahedral

field of the ligands into  $t_{2g}$  and  $e_g$  levels. In the perovskites the average  $t_{2g}-e_g$  splitting is rather well reproduced by a molecular orbital calculation applied to the Ti-O cluster, but fine details—such as bandwidth and relative intensity of the peaks—require a description in terms of one-electron conduction-band DOS. The  $3d$  lowest conduction bands hybridize mainly with the  $2s$  oxygen states located about 17 eV below the top of the valence band and the  $2p$  oxygen states which form the valence band. The  $p-d$  hybridization is particularly strong for the  $e_g$  band whose width is controlled by the  $(pd\sigma)$  two-center integrals.<sup>25</sup> Higher conduction levels are Ti  $4s(a_{1g})$  and  $4p(t_{1u})$  antibonding states lying  $\sim 10$  eV above the bottom of the conduction band. A similar sequence of levels is encountered in titanium carbides and nitrides. For these materials, Neckel *et al.*<sup>11</sup> have recently provided a self-consistent band structure using the APW method. They have computed partial densities of states inside the  $2s$  and  $2p$  carbon and nitrogen and the  $3d$  titanium spheres using a Slater-Koster linear combination of atomic orbitals (LCAO) tight-binding interpolation of APW energy eigenvalues with a total of 41 interaction integrals up to five nearest neighbors. They used the partial densities of states to analyze the metal and

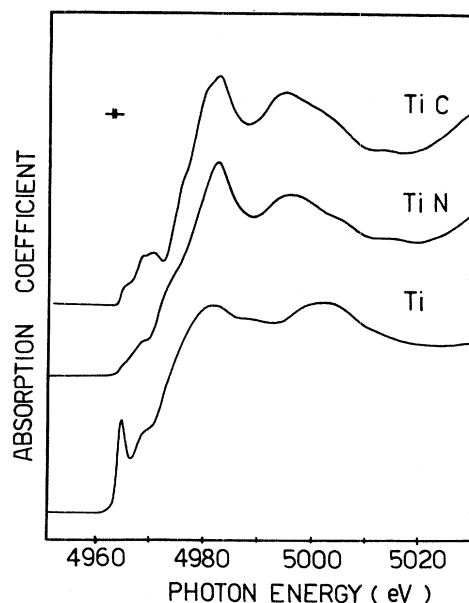


FIG. 2. X-ray absorption near-edge structure (XANES) of Ti in metallic titanium and stoichiometric TiC and TiN. The onset of  $K$  absorption in Ti metal occurs at  $4964.0 \pm 0.5$  eV. In TiC and TiN a chemical shift of  $\sim 1$  eV with respect to pure Ti is observed. The estimated experimental resolution around 5 keV is better than 0.5 eV.

nonmetal x-ray emission spectra of titanium and vanadium carbides, nitrides, and oxides.<sup>35</sup> The agreement was qualitatively good for  $K$  and  $L$  spectra provided the appropriate local density of states inside the metal and nonmetal atomic sphere was used.

Here we follow a similar approach for Ti  $K$ -shell absorption in Ti metal, TiC, and TiN. The absorption coefficient  $\mu_K(E)$  can be written as

$$\mu_K(\omega) = C \omega |M_{\text{Ti}}(p, 1s, E)|^2 \times N_p^{\text{Ti}}(E) \delta(E - E_{1s} - \hbar\omega) \Gamma, \quad (1)$$

where  $M_{\text{Ti}} = \langle 1s | \vec{\epsilon} \cdot \vec{r} | p \rangle$  is the dipole transition matrix element between the Ti  $1s$  core state and the partial  $p$ -like orbitals of the conduction band.  $N_p^{\text{Ti}}(E)$  is the local  $p$ -like DOS (character density of states) giving the number of electron states with  $l=1$  per unit energy and unit cell at energy  $E$  which reside in the Ti sphere. In the APW scheme, the partial DOS is given by<sup>11</sup>

$$N_p^{\text{Ti}}(E) = \sum_{n, \vec{k}} g(n, \vec{k}) q_p^{\text{Ti}}(n, \vec{k}) \delta(E_{n, \vec{k}} - E), \quad (2)$$

where the double sum runs over all the empty electron states  $(n, \vec{k})$  of degeneracy  $g(n, \vec{k})$  and energy  $E_{n, \vec{k}}$ .  $q_p^{\text{Ti}}(n, \vec{k})$  is a weighting factor for the DOS giving the probability of finding a  $p$  electron (due to the dipole selection rule) in the muffin-tin sphere centered on Ti. The finite lifetime of the core hole

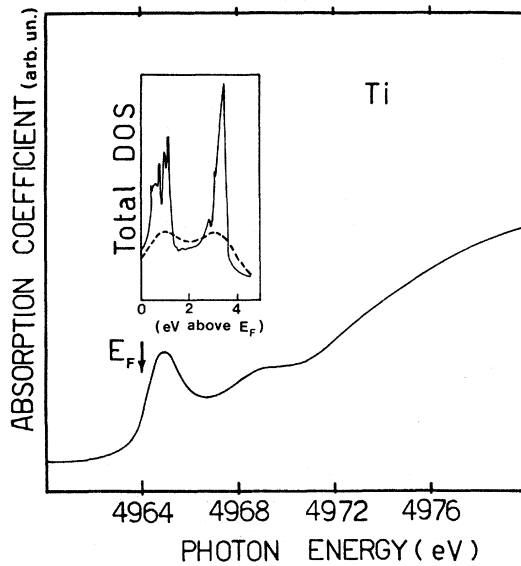


FIG. 3. XANES of Ti metal on an expanded scale. The total mainly- $d$ -like DOS calculated by Jepsen (Ref. 37) is shown in the inset. The dashed curve represents the convolution with a Lorentzian function with a FWHM of 1.3 eV.

is taken into account in Eq. (1) through an energy-independent  $\Gamma$  factor determined by the radiative and not radiative Auger decay (0.9 eV) of the core hole<sup>36</sup> and instrumental resolution.

In Figs. 3–5 we plot the threshold in an expanded scale together with the total and partial  $p$ -like DOS's of the lowest conduction band for TiC and TiN, taken from Neckel *et al.*<sup>11</sup> as well as the total DOS of Ti calculated by Jepsen.<sup>37</sup> The dashed curves are obtained after convolution with a Lorentzian function with a full width at half maximum (FWHM) of 1.3 eV. We take the transition matrix elements to be constant considering that for vanadium carbide the computed transition probability  $|M_V(p, 1s, E)|^2$  is only slightly dependent on energy.<sup>38</sup> Moreover, the  $K$  edges of the first-row transition metals do not exhibit the strong resonance known as a “white line” which occurs, for instance, at the As, Se, and Ge  $K$  edges. On the other hand, the  $L$  edge of titanium metal displays such a resonance.<sup>39</sup> The origin of these resonances is not completely understood, being due to atomic shape resonances, cage effects, or partial density of states.<sup>40</sup>

We can see from Figs. 4 and 5 that the partial DOS describes rather well the peaks of the  $3d$ -like

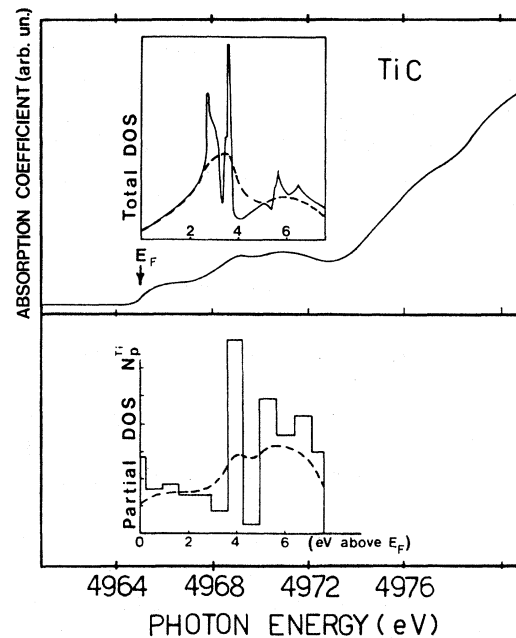


FIG. 4. XANES of TiC on an expanded scale (solid curve). The upper and lower insets show the total and partial  $N_p^{\text{Ti}}(E)$   $p$ -like DOS, respectively, after Neckel *et al.* (Ref. 11). The two curves are not drawn on scale. For their relative intensities, see Fig. 9. The dashed curves are as in Fig. 3.

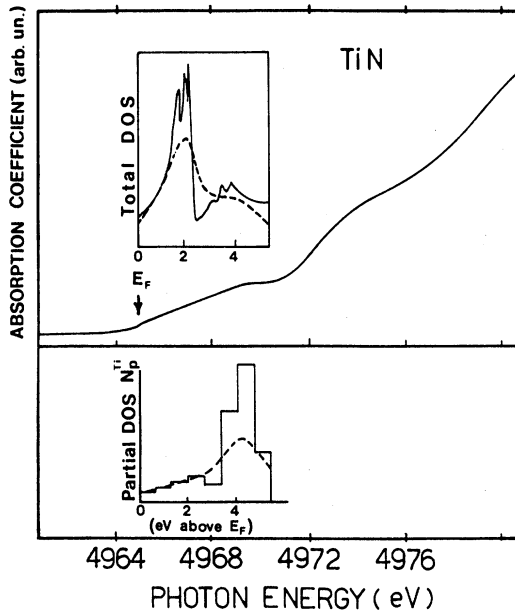


FIG. 5. XANES of TiN on an expanded scale (solid curve). The upper and lower insets show the total and partial  $N_p^{Ti}(E)$   $p$ -like DOS, respectively, after Neckel *et al.* (Ref. 11). The two curves are not drawn on scale. For their relative intensities, see Fig. 10. The dashed curves are as in Fig. 3.

bands which extend from approximately 5.5 and 8 eV above  $E_F$  in TiN and TiC, respectively, in close agreement with band calculations.<sup>11</sup> These bands are reproduced in Figs. 6 and 7. They show the C(N)  $2s$ -filled states lying between 8.8 and 12.1 eV in TiC and between 14.4 and 16.8 eV in TiN. The C(N)  $2p$ -derived bands extend to  $\sim 6$  eV ( $\sim 8$  eV) below  $E_F$  while Ti  $3d$  and  $4s$  bands are empty and form upper conduction states. The higher bands of TiC, C  $3s$  and Ti  $4p$ , are those of Trebin and Bross.<sup>8</sup> The dispersion of the electronic states of TiC near critical points or along  $\Gamma$ - $\Delta$ - $X$  and  $\Gamma$ - $\Lambda$ - $L$  lines has been recently measured by Weaver *et al.*<sup>21</sup> with angle-resolved photoemission. They found results in good agreement with the theoretical bands<sup>11</sup> within 0.5–1 eV. The extremal energies of the C  $2s$  band are, however, deeper than those calculated by about 1 eV. Comparison of the main experimental peaks of Fig. 2 with the theoretical bands allows to correlate qualitatively the features to the average position of the upper unoccupied bands up to about  $\sim 20$  eV from  $E_F$  in TiC and  $\sim 12$  eV in TiN. The shoulder in both compounds corresponds to transitions concerned with Ti  $4s$  bands, while the strong peak at 4982 eV in TiC is mainly related to Ti  $4p$  bands and, partially, to C  $3s$  bands. A similar correlation has been attempted

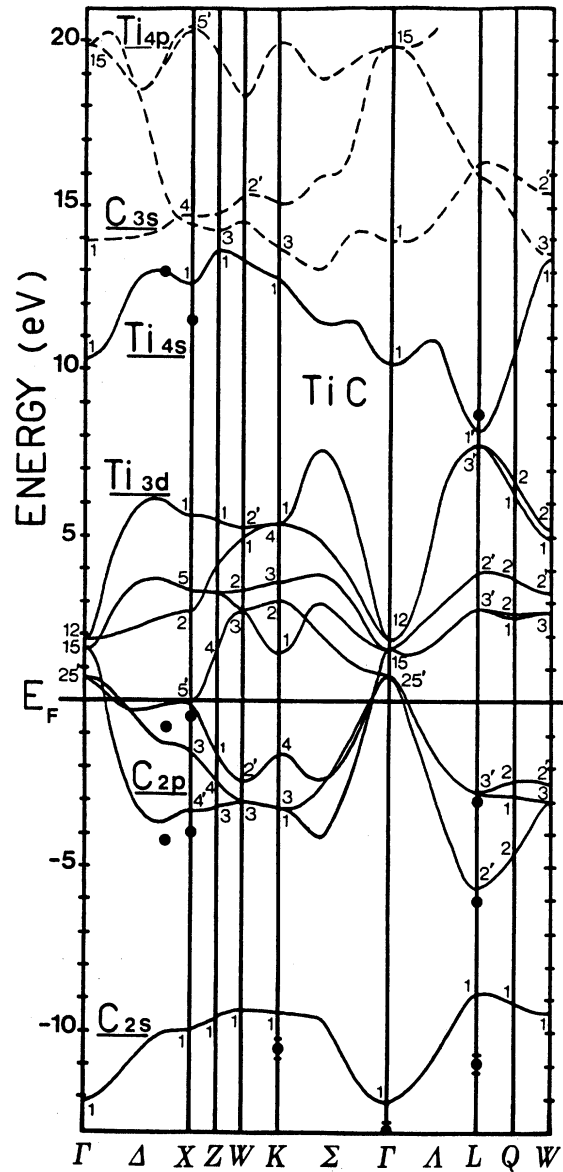


FIG. 6. APW self-consistent valence and conduction bands of TiC after Ref. 11 at high-symmetry points and along high-symmetry lines of the Brillouin zone. The dashed bands are those of Trebin and Bross (Ref. 8). Full circles indicate the angular photoemission data of Weaver *et al.* (Ref. 21). The zero of the energy scale is at the Fermi level.

by Ihara *et al.*<sup>10</sup> for TiC on the basis of their own band calculation.

### B. Relaxation effects

Until now we have confined ourselves to an independent electron model which, at least insofar as  $K$ -shell near-edge excitations are concerned,<sup>25</sup>

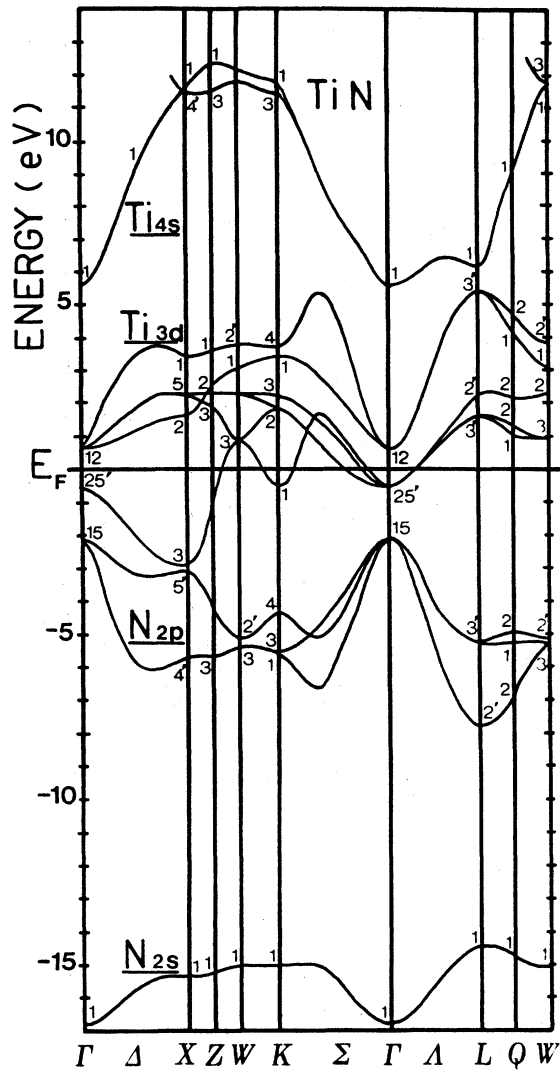


FIG. 7. APW self-consistent valence and conduction bands of TiN after Ref. 11. The zero of the energy scale is at the Fermi level.

seems capable of providing a coherent picture of the lowest empty DOS's in these compounds. Many-body effects, such as relaxation of conduction electrons and edge singularities,<sup>41</sup> due to the presence of the core hole are neglected. To investigate to what extent this approximation is valid in transition metals, we consider x-ray photoelectron spectra (XPS), *K* and *L* emission (XES), and absorption (XAS) spectra for Ti, TiC, and TiN. We anticipate that the screening efficiency of the core hole depends on the amount of electron charge at  $E_F$ , i.e., on the density of occupied states  $N(E_F)$ .

In Figs. 8–10 we have collected the *2p* XPS (Ref. 16), the  $L_{II,III}$  (Refs. 13–15) and  $K\beta_5$  (Ref. 12) emission spectra, the  $L_{II,III}$  XAS of Ti,

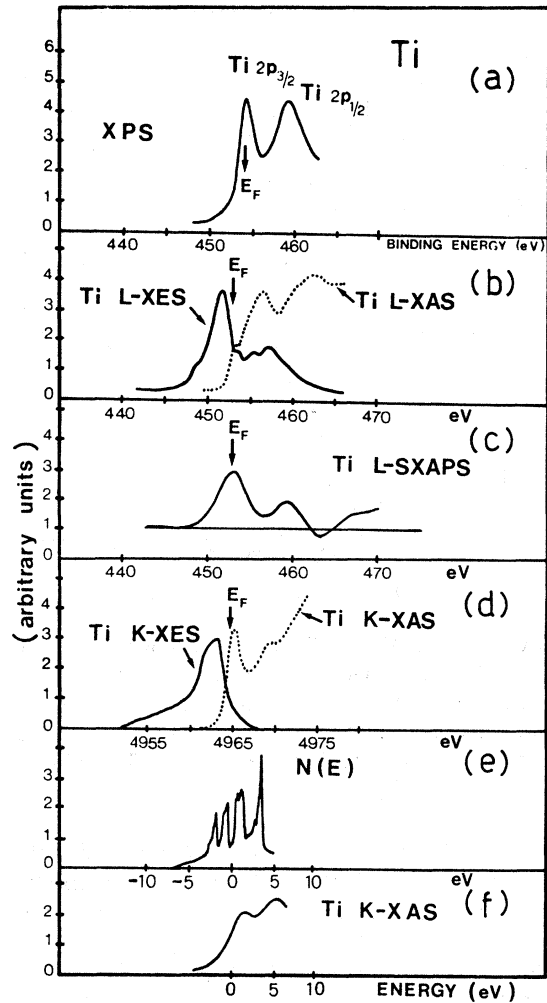


FIG. 8. Juxtaposition of (a) x-ray photoemission, (b)  $L_{II,III}$  emission and absorption, (c) appearance potential, (d) *K* emission and absorption of Ti metal after different sources. The *K*-edge absorption curve is the same as in Fig. 3. (e) and (f) curves represent the total DOS calculated by Jepsen (Ref. 37) and the *K*-edge absorption of Ti in TiFe (Ref. 65), respectively.

TiC, and TiN (Ref. 15) measured by several authors and our *K*-absorption spectra. For Ti we have also included the  $L_{II,III}$  soft-x-ray appearance potential spectrum (SXPAS) measured by Konishi and Kato.<sup>42</sup> The position of the  $L_{III}$  peak corresponds well to the onset of the *L* XAS and marks the position of the lowest conduction band. It is also seen that the edges of the *L* XAS and XES lie at smaller binding energies than the corresponding  $Ti\ 2p_{3/2}$  peak determined by XPS. This energy shift is not the same in all compounds but decreases from TiC to TiN to Ti.

The threshold for absorption and emission oc-

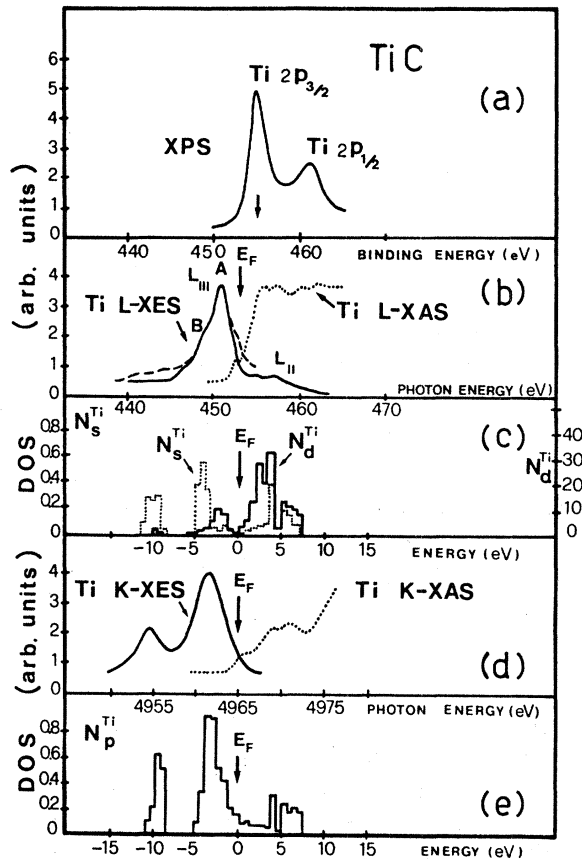


FIG. 9. Juxtaposition of (a) x-ray photoemission, (b)  $L_{II,III}$  emission and absorption, (d)  $K$  emission and absorption of Ti in TiC after different sources. (e) and (c) histograms are the theoretical  $N_p^{Ti}(E)$  and  $N_s^{Ti}(E)$ ,  $N_d^{Ti}(E)$  partial DOS (states/Ry unit cell, Ref. 11). The  $K$ -edge absorption curve is the same as in Fig. 4. The zero of the energy scale in (e) and (c) is placed at the emission edge, as discussed in the text.

occurs at the relaxed energy, since the excited electron moves slowly enough from the ion core that the final-state electrons have time to relax around the hole.<sup>43</sup> The resulting hole potential can thus be imagined to be turned on adiabatically. On the other hand, the relaxation of the  $L_{II,III}$  hole potential is fast, being due to a Koster-Kronig Auger decay mechanism of  $L_{II,III}VV$  type that we will consider in greater detail later. The sudden filling of the hole is accompanied by the emission of satellites from double- or multiply-ionized atoms,<sup>15,44</sup> as can be seen in Figs. 8–10.

In the photoelectron emission the ejected electron has energy in excess of 1 keV with respect to the binding energy of  $2p$  electrons<sup>16</sup> and the hole potential is thus switched on suddenly. The electron leaves swiftly leaving the core ion in an excit-

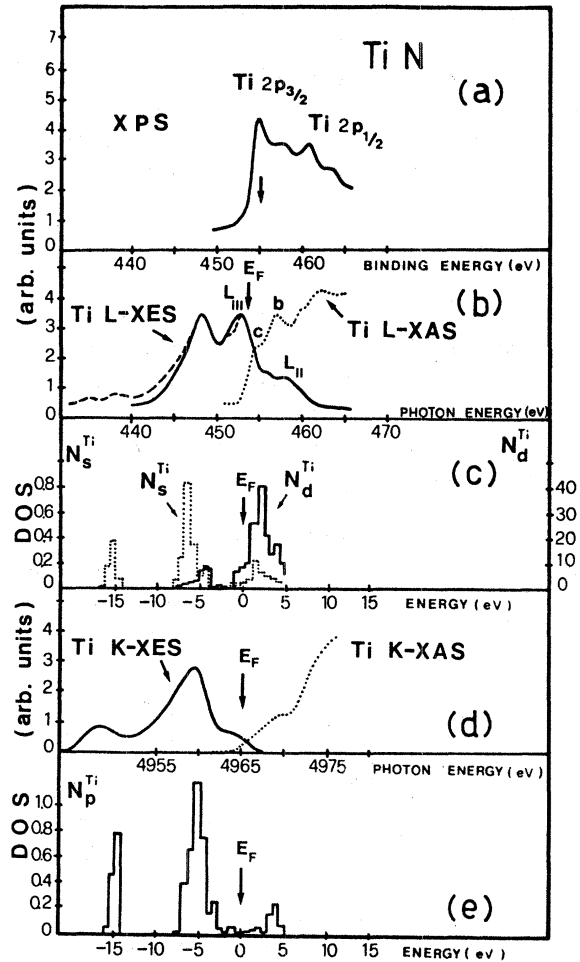


FIG. 10. Juxtaposition of (a) x-ray photoemission, (b)  $L_{II,III}$  emission and absorption, (d)  $K$  emission and absorption of Ti in TiN after different sources. (e) and (c) histograms are the theoretical  $N_p^{Ti}(E)$ ,  $N_s^{Ti}(E)$ , and  $N_d^{Ti}(E)$  partial DOS (states/Ry unit cell, Ref. 11). The  $K$ -edge absorption curve is the same as in Fig. 5. The energy scale zero of (e) and (c) is placed at the emission edge, as discussed in the text.

ed state. The spectrum is composed of discrete shake up peaks satellites lying above the adiabatic threshold energy. These satellites in solids merge in a continuous tailing off<sup>45</sup> above the threshold. This process has been first observed in neon gas<sup>46</sup> by exciting the  $1s$  states with 1.5-keV x-rays and measuring the distribution of charged ions. The photoelectron line shape is asymmetric<sup>45</sup> with an asymmetry index  $\alpha$  depending upon the switching-on time of the hole potential.<sup>47</sup> The peak intensity of the XPS line is not at the  $2p$  core-state binding energy (relative to  $E_F$ ),  $E_{2p}^{\text{peak}} = \hbar\omega - E_{\text{kin}} - \vartheta$ , where  $\vartheta$  is the emitter work function. Because of the sum rule on the response Green's function of

the system,<sup>48</sup> the position of the photoelectric line (first momentum) is at the frozen (unrelaxed) energy in the sudden approximation. An intimate connection may then exist between the presence of satellites and the relaxation shift. Then in the sudden limit the peak energy is shifted towards higher binding energies by a quantity<sup>47</sup>

$$\Delta = -\Gamma \cot[\pi/(2-\alpha)], \quad (3)$$

where  $\alpha = 2(\delta/\pi)^2$  is the  $s$ -wave scattering phase shift (higher  $l$  partial components are neglected for simplicity) of plane wave electrons at  $E_F$  and on the lifetime of the core hole  $\Gamma$ . Thus the "apparent" binding energy depends strongly on the scattering potential of the hole. As discussed by Gadzuk and Šunjić,<sup>47</sup> the finite hole lifetime produces a core-state broadening which forces to average over the shakeup energy distribution, resulting in a centroid of the spectrum displayed to higher binding energies. For  $\delta \approx \pi/2$ , displacements  $\Delta$  as large as  $\Gamma$  can be obtained.<sup>49</sup>

The energy difference between the peak energy of the XPS lines and the Fermi energy position, determined by the onset of the  $L$  absorption and emission, is shown in Fig. 11 as a function of the total, mainly  $d$ -like density of occupied states at  $E_F$ . In Table I we have reported the energies of the main  $L$  absorption peaks including those of TiO and the total DOS after Neckel *et al.*<sup>11</sup> The decrease of  $\Delta$  with increasing the DOS at  $E_F$  indicates that this shift is connected to the availability of flowing charge at  $E_F$ , as also suggested by Eq. (3), since the threshold exponent  $\alpha$  is inversely proportional to the DOS function at the Fermi level.<sup>50,51</sup>

We emphasize that this dynamical relaxation shift could be of relevance while employing XPS to determine the Fermi-level position and then the binding energy of core excitons in semiconductors. In the case of Si a large spread of binding energies ranging from 100 to 900 meV has been reported.<sup>52</sup>

We explicitly notice that the  $L$  absorption edge is sharp, while the  $K$  edge is rounded, suggesting the possibility of a Mahan–Nozières–De Dominicis infrared singularity.<sup>41,53</sup> This occurrence seems likely in view of the creation of  $e$ - $h$  pairs at the Fermi surface following the switching of the  $L_{II,III}$  core hole. Many-body interactions at the  $L$  emission threshold have been studied both experimentally<sup>54</sup> and theoretically<sup>55</sup> in simple metals. However, the sharpening of the emission edge is hard to observe because of the comparatively short lifetime of the hole due to incomplete relaxation<sup>56</sup>

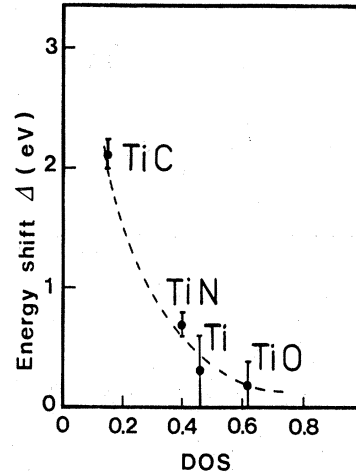


FIG. 11. Energy difference  $\Delta$  between the peak energy of XPS lines and the Fermi energy position determined by the onset of the  $L$  absorption and emission edges for Ti, TiC, TiN, and TiO. The DOS (states per spin/eV unit cell) are those computed in Ref. 11.

or phonon broadening.

Quite recently, experimental evidence of many-body relaxation in the final state on the  $L$  x-ray emission, absorption, and photoelectron spectra of some vanadium compounds has been reported by Curelaru *et al.*<sup>57</sup> and discussed in terms of dynamical screening of the deep hole. In semiconducting vanadium pentoxide  $V_2O_5$  the outer electronic states, both occupied and empty, are deepened 4 eV below  $E_F$  when a core hole is created on the  $V P_{3/2}$  states. The electronic relaxation in the final state (exciton shift) is explained in terms of the Lang-Williams-Kotani-Toyozawa<sup>58–60</sup> mechanism, which is effective in those cases where highly-localized empty levels exist near  $E_F$ , as in rare earths and transition metals. For semiconductors and wide-gap insulators, these localized levels do not become filled on the time scale of the experiment. Thus it is possible to find the XPS edge, corresponding to empty pull down levels, above the absorption and emission edges, which correspond to direct excitation or emission from those levels.

The above analysis indicates that the Fermi energy position has to be located at the intersection between the  $L$  emission and absorption edges, which thus correspond to fully screened holes in the final state of the excitation. One can notice from Figs. 8–10 that this choice for  $E_F$  brings the partial DOS peaks for valence and conduction levels in close agreement with the experimental features of the  $K$  and  $L$  XES and XAS in all compounds.

The  $K$ -edge absorption has been considered

TABLE I. Main peaks of the  $L_{II,III}$  absorption after Ref. 15. The density of states (electron states per spin/eV unit cell) of TiC, TiN, and TiO are those of Ref. 11. All energies are in eV.

	Ti	TiC	TiN	TiO
<i>a</i>	452.8±0.3	452.3	453.7	453.6
<i>b</i>	453.5±0.3	453.0	454.6	454.6
<i>c</i>	456.2±0.3	456	457	456.5
$E_F^a$	453.8	455.1±0.1	455.3±0.2	454.8±0.2
DOS	0.456 <sup>b</sup>	0.14	0.40	0.62

<sup>a</sup>After Ref. 16.

<sup>b</sup>After Ref. 37.

above. Let us discuss the  $L_{II,III}$  emission spectrum of TiC. The  $L_{III}$  emission intensity can be expressed as<sup>61</sup>

$$I_{L_3}(\omega) = C\omega^3 \left[ \frac{1}{3} |M_{Ti}(s, 2p, E)|^2 N_s^{Ti}(E) + \frac{2}{3} |M_{Ti}(d, 2p, E)|^2 N_d^{Ti}(E) \right] \times \delta(E - E_{2p_{3/2}} - \hbar\omega), \quad (4)$$

where  $|M_{Ti}(l, nl', E)|^2$  denotes the transition probability for the  $s$ -like and  $d$ -like components of the valence wave functions, and  $N_s^{Ti}(E)$  and  $N_d^{Ti}(E)$  are the corresponding local partial DOS forming the valence states. To account for the lifetime of the core  $2p$  state we have assumed that a Koster-Kronig Auger mechanism is the main source of that lifetime. In Ti (Ref. 62) and titanium carbides,<sup>18</sup> the  $L_{II,III}$  spin-orbit splitting is large,  $6.1 \pm 0.1$  eV, as seen from the XPS spectra. This means that when a core hole is created at the  $L_{II}$  level of Ti and moves to the  $L_{III}$  level, the energy

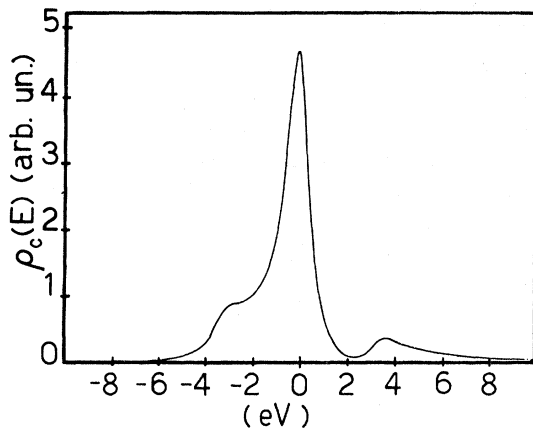


FIG. 12. Auger core density of states  $\rho_c(E)$  according to Watts's theory (Ref. 63). The satellite peaks correspond to plasmon loss and gain at  $\pm\omega_p = 3.23$  eV.

to be released is large enough to create a sizable number of  $e$ - $h$  pairs and plasmons at the Fermi surface. The resulting emission edge broadening can be described by a parameter  $\Gamma(E)$  proportional to the average number of Auger electrons excited by the hole decay, i.e.,

$$\Gamma(E) = b \int \int \rho(E'') \rho(E' - E'') \times \rho_c(E - E') dE' dE'', \quad (5)$$

where, according to Watts,<sup>63</sup>  $\rho_c(E - E')$ , the core DOS function, contains the coupling of the excited electron to the plasmon modes. This function, calculated for TiC, is displayed in Fig. 12. We have used  $\omega_p = 3.23$  eV for the plasmon frequency and lifetime, as determined by Alward and Fong by reflectivity measurements<sup>9</sup> and a plasmon lifetime  $\gamma_p = 0.6$  eV.<sup>64</sup> This kind of dynamical screening is

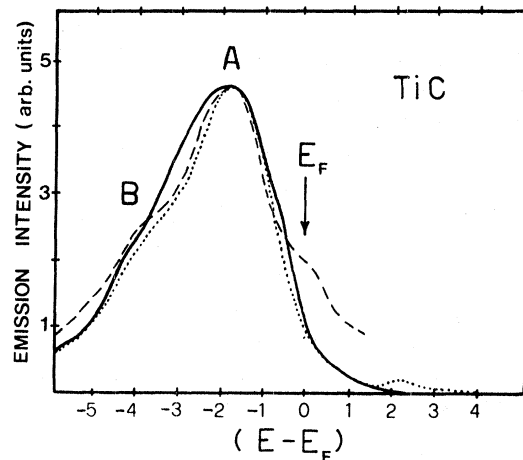


FIG. 13. Comparison between the calculated  $L_{III}$  emission intensity of Ti in TiC (solid line) with the experimental curves from Fischer (Ref. 13, dotted) and Fischer and Baun (Ref. 15, dashed). The zero of the energy scale is at the Fermi edge.

effective when the lifetime of the core is comparable to that of the plasma oscillation of the conduction electrons. In this case the electron gas is still in disequilibrium when the Auger transition takes place. The Auger distribution consists of a central peak and two satellites corresponding to the emission and absorption of plasmons.

The emission intensity is then calculated by convoluting<sup>61</sup>  $I(E)$  from Eq. (4) with  $\Gamma(E)$  from Eq. (5):

$$I_{L_3}(E) = \frac{1}{\pi} \int_0^{E_F} \frac{I(E')\Gamma(E')/2}{(E-E')^2 + [\Gamma(E')/2]^2} dE' \quad (6)$$

As before, the transition probability is taken con-

stant in first approximation. The intensity distribution resulting from Eq. (6) is plotted in Fig. 13 and is compared with the emission data of Fischer<sup>13</sup> and Fischer and Baun.<sup>15</sup> It appears clearly that peak *A* is related to the *d*-like density of states  $N_d^{\text{Ti}}(E)$  whereas shoulder *B* is associated with  $N_s^{\text{Ti}}(E)$ . The overall bandwidth is also in fairly good agreement with experiment. Most of the features discussed for TiC should also be found in TiN and Ti. In the latter case the correspondence between theory and experiment cannot be checked because partial DOS calculations are lacking. In the case of intermetallic TiFe such calculations have been performed for the 3*d* conduction levels<sup>65</sup> and the comparison with the *K*-absorption edge data (Fig. 8) is satisfying.

#### IV. EXAFS REGION

Extended x-ray absorption fine structure has proven to be a rather accurate technique to determine interatomic distances and coordination numbers.<sup>66</sup> The modulation of the atomic absorption coefficient  $\chi(k)$  is caused by the interference between the direct and backscattered electron waves at the atomic sites. In the simplest single-scattering approximation for *K*-shell excitation  $\chi(k)$  has the well-known expression<sup>67</sup>:

$$\chi_i(k) = \frac{4\pi}{k} \sum_j \rho_j \int_0^\infty g_{ij}(r) e^{-2r/\lambda} e^{-2\sigma_{ij}^2 k^2} \sin[2kr + \Phi_{ij}(k)] |f_j(k, \pi)| dr, \quad (7)$$

where  $g_{ij}(r)$  is the radial distribution function for the (*ij*) pair,  $\Phi_{ij}(k) = 2\delta_i(k) + \varphi_j(k) - \pi$  is the total phase shift of the *p*-photoelectron wave propagating from the absorber (*i*) to the backscatterer (*j*) and vice versa,  $|f_j(k, \pi)|$  is the amplitude of the backscatterers,  $\sigma_{ij}^2$  is the thermal Debye-Waller factor, and  $\lambda(k)$  is the mean free path of the photoelectron which describes the damping of the electron wave function due to inelastic scattering processes.  $\rho_j$  is the mean density of the *j*th backscatterer in the sample.

Several refinements to the one-electron picture have been introduced to include the electronic correlation,<sup>27</sup> the intra-atomic relaxation of the orbitals,<sup>68</sup> and the dynamic screening of the core hole.<sup>30</sup> Moreover, the applications of Eq. (7) to the case of strongly disordered<sup>69,70</sup> or anisotropic systems<sup>71</sup> has also been made. All these corrections aim to establish the quantitative limitations of the technique and its applicability to different systems. The processing of the data also involve subtle problems which have been discussed recently.<sup>72</sup>

In order to obtain reliable distance information from EXAFS oscillations, one needs correct phase functions  $\Phi_{ij}(k)$  and amplitudes  $f_j(k, \pi)$ . The best  $\Phi_{ij}(k)$ 's and  $f_j(k, \pi)$ 's available to date are those calculated by Teo and Lee<sup>31</sup> using Clementi-Roetti

and Herman-Skillman atomic wave functions. It is generally believed that they are good enough to provide accurate values for the bond lengths, particularly for intermediate-*Z* atoms.

The Fourier transform of  $\chi(k)$  yields the radial distribution function  $F(R)$  around the absorbing atom,<sup>67</sup> i.e.,

$$F(R) = \frac{1}{\sqrt{2\pi}} \int_{k_{\min}}^{k_{\max}} dk e^{-2ikr} k^n \chi(k) W(k), \quad (8)$$

where the integral is taken over a finite *k* interval, typically  $\Delta k = k_{\max} - k_{\min} = 12 \text{ \AA}^{-1}$ .  $W(k)$  is a window function, usually a Gaussian function, which reduces side lobes caused by termination effects on  $\chi(k)$ . Because of the phase shift  $\Phi_{ij}(k)$  in the argument of the sine function in Eq. (7), interatomic distances derived from the peaks of  $F(R)$  have to be properly corrected to coincide with those of x-ray diffraction.

The zero of the energy (momentum) scale has often to be changed by parametrizing the reference energy  $E_0$  defined as

$$E_0 = \hbar\omega - \frac{\hbar^2}{2m} k^2. \quad (9)$$

The choice of  $E_0$  is made on the basis of the Lee and Beni<sup>27</sup> criterion, which requires that the mag-

nitude  $F(R)$  and the imaginary part of the normalized Fourier transform of  $\chi(k)e^{-i\Phi_{ij}(k)}$  should peak at the same distance, or on the prescription that the bond lengths  $R_j$  should be independent on the kinetic energy of the photoelectron.<sup>73</sup> By letting  $E_0$  vary, the measured distances  $R_j$  could be made coincident with x-ray diffraction data within 0.02 Å or better. Both procedures are essentially equivalent but their use may mask possible relaxation effects, since  $\Delta\Phi_{ij}(k) = 2R_{ij}\Delta E_0/k$  (Ref. 27) and thus changes in  $E_0$  affect largely  $\Delta\Phi_{ij}(k)$  at small  $k$ , where electronic relaxation is important. Hence in those systems in which sizable electron screening is envisaged, the wave-vector dependence of  $\Phi_{ij}(k)$  must be considered with care. In the following we will analyze the EXAFS of Ti, TiC, and TiN  $K$  spectra with the above considerations in mind.

#### A. Titanium

The absorption above the Ti  $K$  edge after pre-edge subtraction is shown in Fig. 14. The EXAFS function  $k\chi(k)$  of Ti is derived from the corresponding spectrum using the usual procedure and is plotted in Fig. 15(a). The Fourier transform of  $k\chi(k)$  yields the amplitude of the radial distribution function  $F(R)$  around each Ti atom, which is also plotted in Fig. 15(b). The  $F(R)$  of hcp Ti in Fig. 15(b) consists of a main peak located at  $2.52 \pm 0.01$  Å which corresponds to two nearest-neighbor titanium subshells of six atoms located at

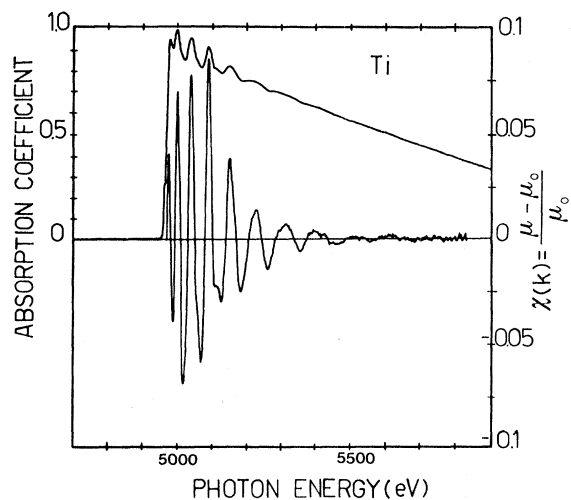


FIG. 14. Experimental Ti  $K$  absorption spectrum after pre-edge subtraction and extracted EXAFS modulation  $k\chi(k)$ .

2.889 and 2.940 Å, respectively.<sup>74</sup> The following peaks are the third, fourth, and fifth shells located at 3.87, 4.68, and 5.46 Å. The position of the first shell differs somewhat from that found by Denley *et al.*<sup>39</sup> from the analysis of the  $L$  edge,  $R = 2.672$  Å, mainly because of the smaller contribution of the central atom  $2\delta^{(0)}(k)$  and  $2\delta^{(2)}(k)$  terms to the total phase shift  $\Phi_{ij}$ .

In the hcp structure the third, fourth, and fifth shells have intensities consistently weaker compared to the first shell than in fcc structure where the central atom is also surrounded by twelve neighbors. This behavior might be related to the high degree of shadowing around the central atom due to the compactness of the hcp lattice. Accordingly,  $k\chi(k)$  in Fig. 15(a) is basically built from a single frequency.

We have applied the Teo and Lee criterion to find  $E_0$  because, according to the results of Sec. III, large relaxation effects do not occur in Ti metal. We have found that the Lee and Beni condition is fulfilled when  $E_0$  is close to the steepest part of the edge of Fig. 14, marking the onset of transitions to the Fermi edge.

By back-Fourier inversion of the first peak of  $F(R)$  between 1.5 and 3.15 Å, we obtain the modulated component  $k\chi(k)$  of the first coordination shell. The envelope function

$$\tilde{A}_j(k) = \frac{N_j |f_j(k, \pi)| e^{-2R_j/\lambda} e^{-2\sigma_j^2 k^2}}{R_j^2}, \quad (10)$$

peaks at  $k = 4.95$  Å<sup>-1</sup> but does not show any beating produced by the two Ti subshells which are separated by  $\sim 0.04$  Å. A model calculation for  $k\chi(k)$  has been done utilizing Teo and Lee amplitudes and phases<sup>31</sup> and assuming a Debye-Waller

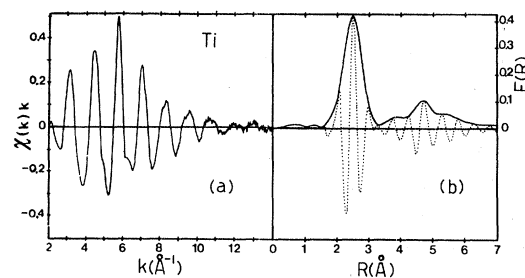


FIG. 15. (a)  $k\chi(k)$  for metallic titanium film. (b) Magnitude  $F(R)$  and imaginary part  $\text{Im}F(R)$  of the Fourier transform of  $k\chi(k)$  vs  $R$ . The integration range is  $k_{\min} = 2.3$  Å<sup>-1</sup> and  $k_{\max} = 14.5$  Å<sup>-1</sup>. A Gaussian window  $W(k)$  is used.

factor,

$$\sigma_{\text{Ti-Ti}}^2 = 2\sigma_\infty^2(1 - \Delta_c), \quad (11)$$

computed within the classical harmonic approximation.<sup>75</sup>  $\sigma_\infty^2 \Delta_c$  describes the correlated motion of the atoms and  $\sigma_\infty^2$  is the mean-square displacement of the individual atoms. The resulting  $k\chi(k)$ , shown in Fig. 16(a), differs from the experimental one for a constant phase shift of about  $\pi/2$  over the whole  $k$  range and for an amplitude factor of 20%. Moreover, the magnitude of the model radial distribution function  $F(R)$ , shown in Fig. 16(b), differs by nearly the same quantity from the experimental  $F(R)$ . This discrepancy might be due, in part, to many-body effects which are left out of the classical formulation of the EXAFS theory.<sup>67</sup> Rehr *et al.*<sup>68</sup> have shown that one-electron calculations overestimate the scattering amplitudes unless a correction is made for the relaxation of the passive electron orbitals. Namely, the single-particle matrix elements have to be scaled by a reduction factor  $S_0^2 \equiv |\langle \phi'_{N-1} | \phi_{N-1} \rangle|^2$ , where  $|\phi'_{N-1}\rangle$  and  $|\phi_{N-1}\rangle$  are the wave functions of the  $N-1$  electrons with and without the core hole, respectively.  $S_0^2$  ranges between 0.6 and 0.9, depending on the atom considered<sup>76</sup> and is generally taken constant and independent on the kinetic energy of the excited electron. Multielectron excitation channels—shake-up and shake-off processes discussed in Sec. III—give an additional correction factor of 10% to the amplitude and modify slightly the phase shift. This phase change may, however, be properly accounted for by shifting the excitation energy zero scale  $E_0$ .

When the experimental phase derived by inverting the  $F(R)$  of the first shell (Fig. 17) is used instead of the Teo and Lee data and a correction factor  $S_0^2 = 0.85$  is applied to the scattering amplitude, the agreement is quite good for both  $\tilde{A}(k)$  and  $F(R)$ , as shown in Fig. 18.

It is interesting to note that the above analysis of hcp Ti does not require the use of an asymmetric  $g_{ij}(r)$  as found by Eisenberger and Brown<sup>71</sup> for hcp Zn. At room temperature the harmonic approximation, implying  $g_{ij}(r) = \delta(r - r_j)$ , is still valid for Ti whose  $c/a$  ratio and Debye temperature are similar to those of Zn. The reason of this discrepancy is not clear yet.

### B. Titanium carbide and nitride

Figure 19 shows the measured  $k\chi(k)$  for TiC and TiN around the Ti  $K$  edge and Fig. 20 the cor-

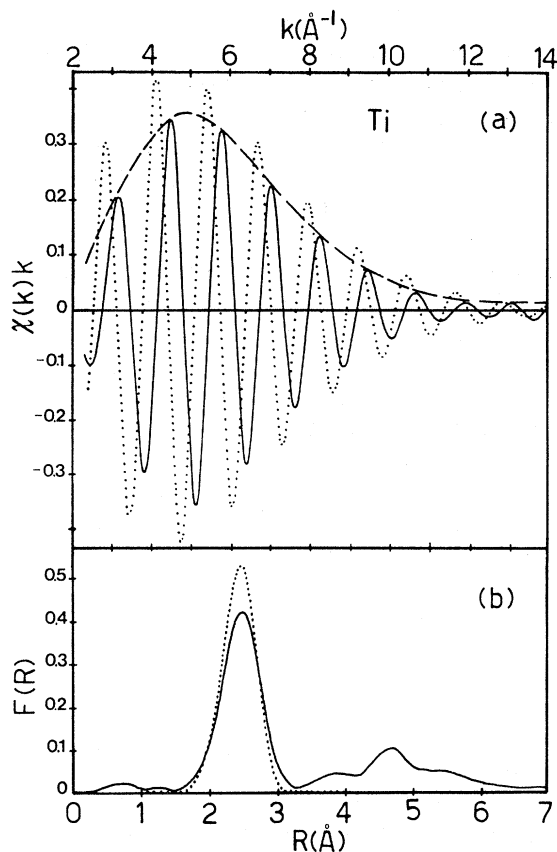


FIG. 16. (a) Back-Fourier transform  $k\chi(k)$  of the first peak of the radial distribution function  $F(R)$  of Ti (solid line) and its envelope function  $\tilde{A}(k)$  (dashed line). The dotted curve is a model  $k\chi(k)$  calculated from Eq. (7), using amplitudes and phases of Teo and Lee (Ref. 31), a Gaussian-type  $g_{ij}(r)$  and  $\sigma^2 = 0.007 \text{ \AA}^2$ . The first two Ti shells, located at  $R_1 = 2.889 \text{ \AA}$  and  $R_2 = 2.940 \text{ \AA}$  (Ref. 74) are considered. (b) Fourier transform  $F(R)$  of the model  $k\chi(k)$  of (a) compared with experimental  $F(R)$ .

responding  $F(R)$ . Placing  $E_0$  at the onset of the  $K$  edge satisfies automatically the Lee and Beni prescription for the first two peaks, as shown for TiN in Fig. 20. The  $\Phi_{ij}(k)$  for the Ti-Ti pair obtained by the back-Fourier procedure is shown in Fig. 21 and compared with the Teo and Lee data.<sup>31</sup> The  $\Phi_{\text{Ti-Ti}}(k)$  for TiC is in excellent agreement with that reported by Moisy,<sup>77</sup> who also takes  $E_0$  at the absorption edge. The comparison with that derived from Ti indicates that the Ti-Ti phase is transferable in these compounds to a high degree of accuracy. However, only qualitative agreement is obtained for the amplitude  $\tilde{A}(k)$ , where an un-

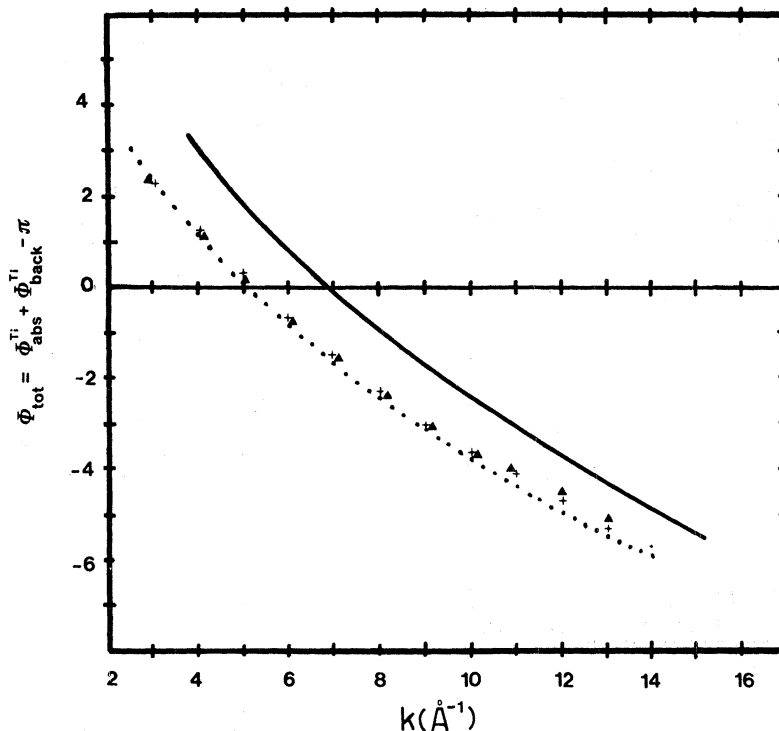


FIG. 17. Total phase shift  $\Phi$  vs  $k$  (in radians) for the Ti-Ti pair in Ti metal (dotted line), TiC ( $\blacktriangle$ ) and TiN ( $+$ ). The Teo and Lee theoretical phase is shown for comparison (solid line).

certainty of about  $1 \text{ \AA}^{-1}$  is seen in the position of the maximum, Fig. 22(b). The reduction factor  $S_0^2$  also differs slightly from that of Ti, being  $S_0^2 = 0.80$  for TiC and TiN.<sup>26</sup> The first peak of  $F(R)$  in Fig. 20 is associated to the shells of six C and N equivalent atoms surrounding the central Ti atom at  $d=2.164$  and  $2.121 \text{ \AA}$ . The third shell of the light elements is barely seen only in TiN because of the larger backscattering power of N atoms with respect to C, shown in Fig. 22(a).

To check the reliability of theoretical phases for light elements, we have computed  $\chi(k)$  of TiN by introducing into Eq. (7) the appropriate phase and amplitude functions of Teo and Lee. Only the first two shells of nitrogen and titanium atoms, which surround the central Ti atom, are considered. The  $F(R)$  is then calculated by Fourier transforming  $k\chi(k)$  between appropriate  $k$  limits. In Fig. 23(a) a comparison is made with the experimental  $F(R)$ . We notice a remarkable disagreement in the position of the nitrogen shell. This disagreement could be due to the fact that theoretical phases for light elements are only approximate. When the same calculation is performed by using the experimental phase and amplitudes of Figs. 21

and 22 the agreement with the model calculations improves substantially [Fig. 23(b)].

To improve the determination of TiC and TiN bond lengths we adopt the beating method. This method was originally developed by Martens

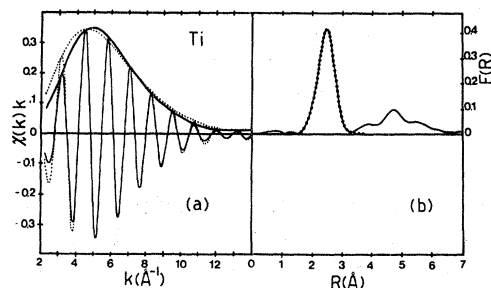


FIG. 18. (a) Model  $k\chi(k)$  and  $\tilde{A}(k)$  (dotted lines) computed from Eq. (7) using the reduced  $S_0^2=0.85$  amplitudes of Teo and Lee (Ref. 31) and experimental phases. The other parameters are as in Fig. 16. The solid curve is the experimental  $k\chi(k)$ . (b)  $F(R)$  deduced from the model  $k\chi(k)$  of (a) (dots) compared with the experimental  $F(R)$ .

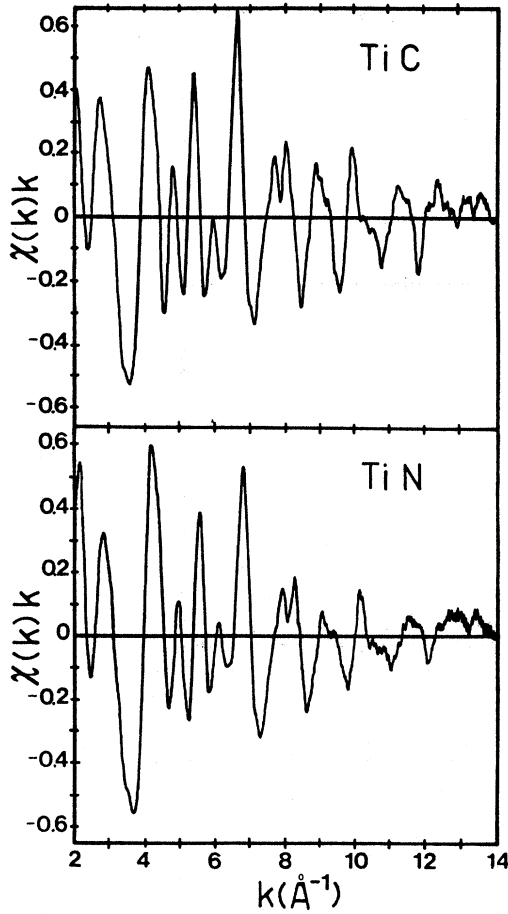


FIG. 19.  $k\chi(k)$  EXAFS modulation of TiC and TiN above the Ti K edge.

*et al.*<sup>78</sup> for two shells containing the same atoms and then extended by Balzarotti *et al.*<sup>79</sup> to different atomic species. The difference  $\Delta R$  in the bond length of two nonequivalent shells is given by

$$\Delta R_{1,2} = \frac{n\pi - [\varphi_2(k) - \varphi_1(k)]}{2k_{\min}^{(n)}} \quad (n = 1, 3, 5, \dots), \quad (12)$$

where  $k_{\min}^{(n)}$  is the minimum of the envelope backscattering function of a given pair of beating shells corresponding to a given  $n$  and  $\varphi_j(k)$  are the values of their backscattering phase shifts.

By taking the back-Fourier transform of  $F(R)$  for TiC and TiN in the 1.0–3.0 Å, we obtain the results shown in Fig. 24. Minima of  $\tilde{A}(k)$  clearly occur at values  $n=3,5,7$  for TiC and  $n=1,3,5,7$  for TiN. The total phase shift of the two beating shells are<sup>31</sup>

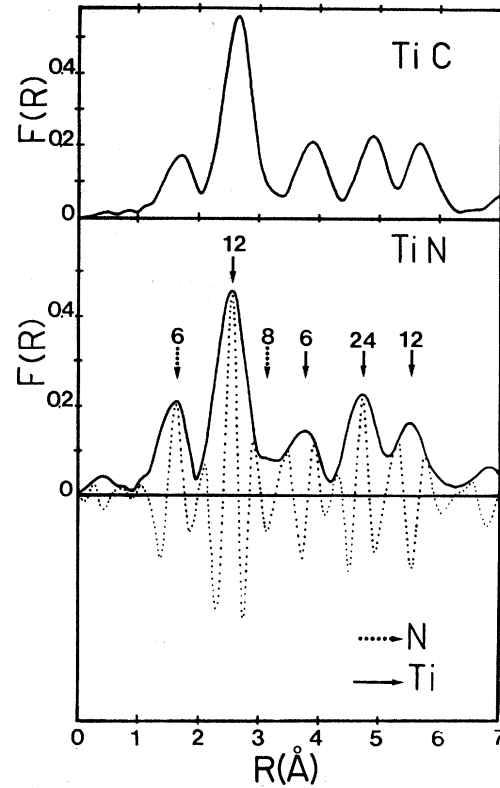


FIG. 20.  $F(R)$  derived from  $k\chi(k)$  of Fig. 19. For TiN the  $\text{Im}F(R)$  function is also shown. The labeled arrows mark the position and the coordination number of the N and Ti atoms in the lattice.

$$\Phi_{\text{Ti1}}(k) = 2\delta^{\text{Ti}}(k) + \varphi_1^{\text{back}}(k) - \pi \quad (1 = \text{C, N}), \quad (13)$$

$$\Phi_{\text{Ti2}}(k) = 2\delta^{\text{Ti}}(k) + \varphi_2^{\text{back}}(k) - \pi \quad (2 = \text{Ti}), \quad (14)$$

where  $2\delta^{\text{Ti}}(k)$  is the central atom (Ti) phase shift. So the phase difference

$$\Phi_{\text{Ti2}}(k) - \Phi_{\text{Ti1}}(k) = \varphi_2^{\text{back}}(k) - \varphi_1^{\text{back}}(k) \quad (15)$$

contains the difference of the backscattering phase only. In Table II we compare the crystallographic data<sup>74</sup> for TiC and TiN with the values of  $\Delta R$  derived from Eq. (12) by using our experimental phases for TiC and TiN and those calculated from Teo and Lee.<sup>31</sup> Agreement with diffraction data is fairly good when the set of experimental phases is used indicating that these low- $Z$  atom phases are reliable.

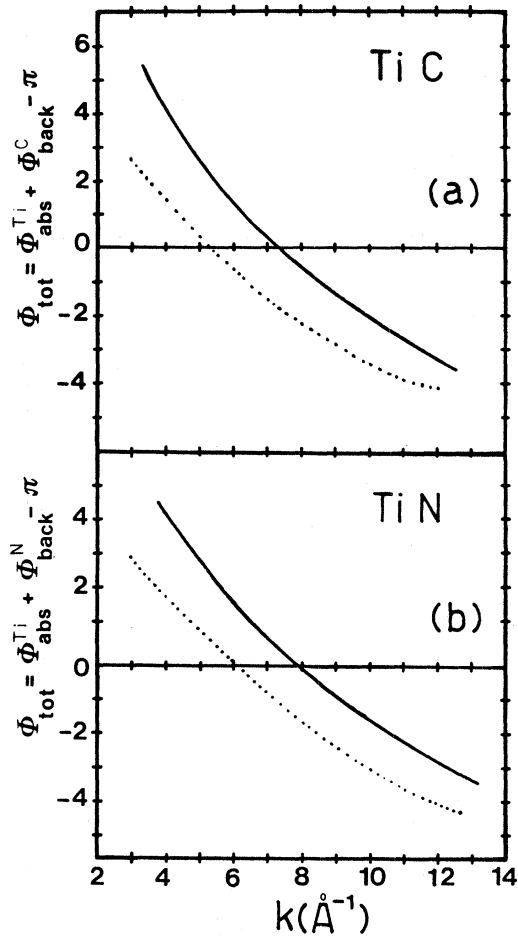


FIG. 21. Experimental phases (a)  $\Phi_{\text{Ti-C}}(k)$  and (b)  $\Phi_{\text{Ti-N}}(k)$  (in rads). The solid lines are the theoretical phases of Teo and Lee.

According to Lee and Beni, the hole created by the absorption of a photon on the Ti atom is always completely relaxed, no matter how the excitation energy is. This limit is equivalent to replace the ion core potential in presence of a core hole with the potential of a  $Z + 1$  ion (equivalent core approximation). The assumption of atomic relaxation of the central atom affects the phase term  $\Phi_{ij}(k)$  through the  $k$  dependence of the  $2\delta(k)$  phase shift. The  $\Phi_{ij}(k)$  solid curves of Figs. 17 and 21 are computed within this approximation. Very recently, effects of the dynamical screened potential on the  $2\delta(k)$  phase shift have been considered theoretically by Noguera and Spanjaard<sup>30</sup> for Al. They showed that the inclusion of a time-dependent scattering potential results in a wave-vector dependence of  $\Phi_{ij}(k)$ , which is inter-

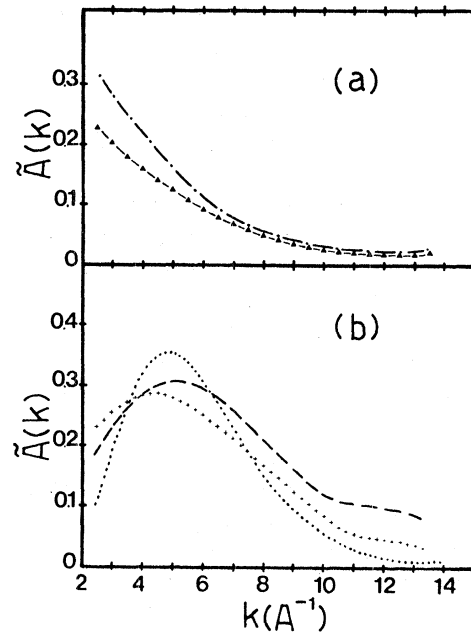


FIG. 22. Experimental amplitudes for (a) C and N (dash-dotted) atoms and (b) Ti in Ti metal (dotted), in TiC (dashed), and in TiN (crosses).

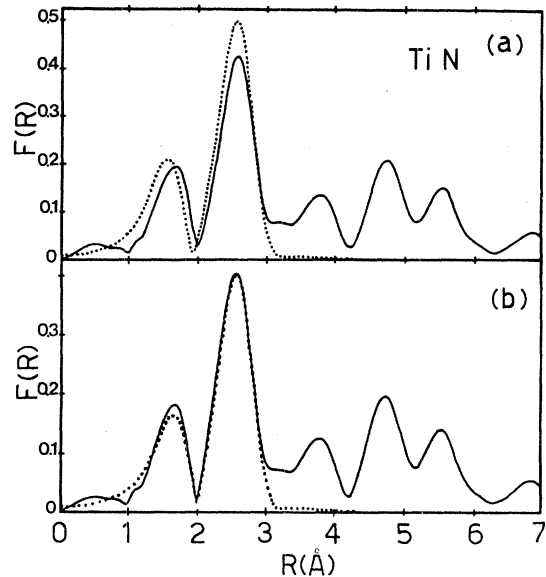


FIG. 23. Comparison of the experimental  $F(R)$  for TiN with (a) model calculations based on Teo and Lee phases and amplitudes, and (b) experimental phases and amplitudes. Only the first two coordination shells (N and Ti) around the central Ti atoms are included.

mediate between that of total unscreened and completely screened case. As expected,  $\Phi_{ij}(k)$  is more screened-like for small  $k$  and approaches the unscreened  $\Phi_{ij}(k)$  at high kinetic energies. Such a trend is displayed by the  $\Phi_{\text{Ti-Ti}}(k)$  in TiC and TiN (Fig. 21) and, to minor extent, in Ti (Fig. 17), where the electronic screening is more efficient, as pointed out in Sec. III A. The difference between the unscreened  $\Phi_{ij}(k)$  (Teo and Lee) and the dynamical screened phase shifts is consistent with the one computed for Al.<sup>30</sup>

In summary, we have shown that sizable electronic screening effects may be detected in 3d transition metals at high kinetic energies of the photoelectron either through the examination of the energy shift of the photoemission lines with respect to the emission edge and the wave-vector dependence of the phase shift of the photoelectron in the EXAFS regime.

#### ACKNOWLEDGMENTS

We are strongly indebted to F. Bassani and G. Strinati for many illuminating discussions and to C. Noguera and Y. Toyozawa for their interest in this work. We are also particularly grateful to F. Comin and S. Mobilio for their contribution to some stages of the work. Thanks are due to F. C. Brown for providing us with a copy of his work prior to publication and to A. Neckel for a copy of an unpublished report. We thank U. La Malfa of the FIAT Research Center for the samples of titanium carbide and nitride. The technical assistance of L. Moretto is gratefully acknowledged.

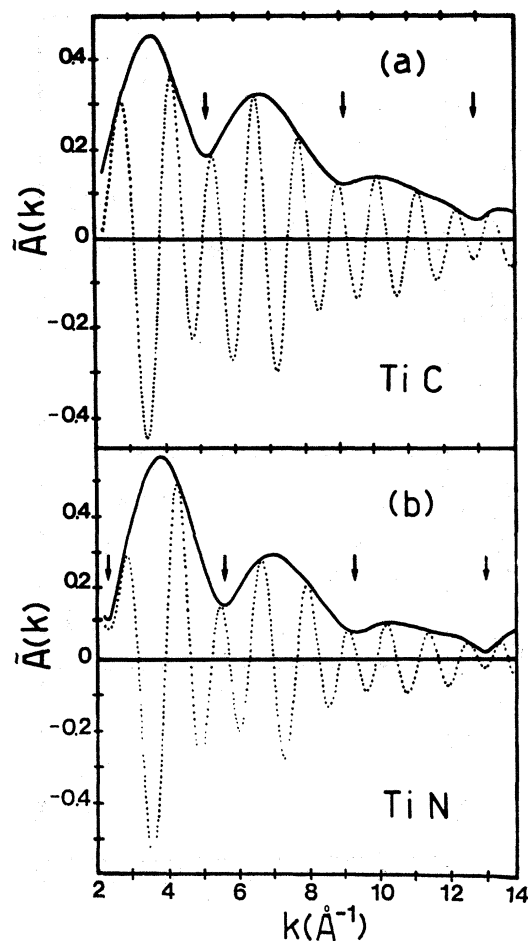


FIG. 24.  $k\chi(k)$  and  $\tilde{A}(k)$  for (a) TiC and (b) TiN obtained by back-Fourier transforming the C and Ti peaks of  $F(R)$  in Fig. 20 between 1 and 3 Å. The beating minima are marked by arrows.

TABLE II. Differences in bond length  $\Delta R_{\text{expt}}$  of two nonequivalent shells of atoms surrounding Ti in TiC and TiN, as determined by the beating method.  $\Delta R_{\text{calc}}$  are the results of a model calculation using Teo and Lee phases (Ref. 31).  $\Delta R_{\text{cryst}}$  are taken from Ref. 74.

	$n$	$K_{\text{min}}^{\circ}$ ( $\text{Å}^{-1}$ )	$\Delta R_{\text{expt}}$	$\Delta R_{\text{calc}}$	$\Delta R_{\text{cryst}}$
TiC	3	5.225	0.899	0.969	
	5	9.125	0.883	0.878	0.896
	7	12.950	0.881	0.868	
TiN	3	5.625	0.885	0.979	
	5	9.425	0.860	0.867	0.879
	7	13.150	0.836	0.871	

- <sup>1</sup>L. E. Toth, *Transition Metal Carbides and Nitrides*, (Academic, New York, 1971), Vol. 7; W. S. Williams, in *Progress in Solid State Chemistry*, edited by H. Reiss and J. D. McCallan (Pergamon, New York, 1971), Vol. 6.
- <sup>2</sup>Ch. H. de Novion and V. Maurice, *J. Phys. C* **7**, 211 (1977).
- <sup>3</sup>E. K. Storms, *The Refractory Carbides* (Academic, New York, 1967).
- <sup>4</sup>P. Z. Ehrlich, *Z. Anorg. Chem.* **259**, 1 (1949).
- <sup>5</sup>V. Ern and A. C. Switendick, *Phys. Rev.* **137**, 1927 (1965), and references therein to earlier work.
- <sup>6</sup>R. G. Lye and E. M. Logothetis, *Phys. Rev.* **147**, 622 (1966).
- <sup>7</sup>J. B. Conklin Jr. and D. J. Silversmith, *Int. J. Quantum Chem.* **25**, 243 (1968).
- <sup>8</sup>H. R. Trebin and H. Bross, *J. Phys. C* **8**, 1181 (1975).
- <sup>9</sup>J. F. Alward, C. Y. Fong, M. El-Batanouny, and F. Wooten, *Phys. Rev. B* **12**, 1105 (1975).
- <sup>10</sup>H. Ihara, Y. Kumashiro, and A. Itoh, *Phys. Rev. B* **12**, 5465 (1975).
- <sup>11</sup>A. Neckel, P. Rastl, R. Eibler, P. Weinberger, and K. Schwarz, *J. Phys. C* **9**, 579 (1976); Report No. SUP 70017 (unpublished).
- <sup>12</sup>L. Ramqvist, B. Ekstig, E. Källme, E. Noreland, and R. Manne, *J. Phys. Chem. Solids* **30**, 1849 (1969).
- <sup>13</sup>D. W. Fischer, *J. Appl. Phys.* **41**, 3922 (1970).
- <sup>14</sup>J. E. Holliday, *J. Phys. Chem. Solids* **32**, 1825 (1971).
- <sup>15</sup>D. W. Fischer and W. L. Baun, *J. Appl. Phys.* **39**, 4757 (1968).
- <sup>16</sup>L. Ramqvist, K. Hamrin, G. J. Johansson, A. Fahlman, and C. Nordling, *J. Phys. Chem. Solids* **30**, 1835 (1969).
- <sup>17</sup>A. L. Hagström, L. I. Johansson, B. E. Jacobson, and S. B. Hagström, *Solid State Commun.* **19**, 647 (1976).
- <sup>18</sup>L. I. Johansson, A. L. Hagström, B. E. Jacobson and S. B. Hagström, *J. Electron. Spectrosc. Relat. Phenom.* **10**, 259 (1977).
- <sup>19</sup>L. I. Johansson, P. M. Stefan, M. L. Shek, and A. N. Christensen, *Phys. Rev. B* **22**, 1032 (1980).
- <sup>20</sup>J. H. Weaver and F. A. Schmidt, *Phys. Lett.* **77A**, 73 (1980).
- <sup>21</sup>J. H. Weaver, A. M. Bradshaw, J. F. Van der Veen, F. J. Himpsel, D. E. Eastman, and C. Politis, *Phys. Rev. B* **22**, 4921 (1980).
- <sup>22</sup>G. Böhm and H. Goretzki, *J. Less-Common Metals* **27**, 311 (1972).
- <sup>23</sup>A. Schlegel, P. Wachter, J. J. Nickl, and H. Lingg, *J. Phys. C* **10**, 4889 (1977).
- <sup>24</sup>D. W. Lynch, C. G. Olson, D. J. Peterman, and J. H. Weaver, *Phys. Rev. B* **22**, 3991 (1980).
- <sup>25</sup>A. Balzarotti, F. Comin, L. Incoccia, M. Piacentini, S. Mobilio, and A. Savoia, *Solid State Commun.* **35**, 145 (1980).
- <sup>26</sup>For a discussion of the dependence of  $S_0^2$  on the excitation electron energy and chemical bonding see E. A. Stern, B. A. Bunker, and S. M. Heald, *Phys. Rev. B* **21**, 5521 (1980).
- <sup>27</sup>P. A. Lee and G. Beni, *Phys. Rev. B* **15**, 2862 (1977).
- <sup>28</sup>E. A. Stern, S. M. Heald, and B. Bunker, *Phys. Rev. Lett.* **42**, 1372 (1979).
- <sup>29</sup>A. Fontaine, P. Lagarde, D. Raoux, and J. M. Esteve, *J. Phys. F* **9**, 2143 (1979).
- <sup>30</sup>C. Noguera and D. Spanjaard, *J. Phys. F* **11**, 1133 (1981).
- <sup>31</sup>B. K. Teo and P. A. Lee, *J. Am. Chem. Soc.* **101**, 2815 (1979).
- <sup>32</sup>A. Balzarotti, F. Comin, L. Incoccia, and S. Mobilio, *Frascati Report No. LNF* (unpublished).
- <sup>33</sup>S. Mobilio, F. Comin, L. Incoccia, *Frascati Report No. LNF* (unpublished).
- <sup>34</sup>B. M. Davies and F. C. Brown, *Phys. Rev. B* **25**, 2997 (1982).
- <sup>35</sup>A. Neckel, K. Schwarz, R. Eibler, P. Rastl, and P. Weinberger, *Mikrochim. Acta Suppl.* **6**, 257 (1975).
- <sup>36</sup>V. O. Kostroun, M. H. Chen, and B. Crasemann, *Phys. Rev. A* **3**, 533 (1971).
- <sup>37</sup>O. Jepsen, *Phys. Rev. B* **12**, 2988 (1975).
- <sup>38</sup>K. Schwarz and A. Neckel, *Ber. Bunsenges. Phys. Chem.* **79**, 1071 (1975).
- <sup>39</sup>D. Denley, R. S. Williams, P. Perfetti, D. A. Shirley, and J. Stöhr, *Phys. Rev. B* **19**, 1762 (1979).
- <sup>40</sup>F. C. Brown, in *Synchrotron Radiation Research*, edited by H. Winick and S. Doniach (Plenum, New York, 1980).
- <sup>41</sup>P. Nozières and C. T. De Dominicis, *Phys. Rev.* **178**, 1097 (1969); G. D. Mahan, *Phys. Rev. B* **11**, 4814 (1975).
- <sup>42</sup>R. Konishi and S. Kato, *Jpn. J. Appl. Phys.* **15**, 1237 (1976).
- <sup>43</sup>The Auger width of the *L* hole is larger than 1 eV (1.22 eV in V) corresponding to  $\tau_A \leq 6.5 \times 10^{-16}$  sec, whereas the radiative decay time is  $\tau_R \cong 3 \times 10^{-13}$  sec. The relaxation time of conduction electrons is therefore much shorter than the radiative lifetime which is comparable to that of a typical lattice vibration.
- <sup>44</sup>C. Bonnelle, *Ann. Phys. (Paris)* **1**, 439 (1965).
- <sup>45</sup>S. Doniach and M. Šunjić, *J. Phys. C* **3**, 285 (1970).
- <sup>46</sup>T. A. Carlson and M. D. Krause, *Phys. Rev.* **140A**, 1057 (1965).
- <sup>47</sup>J. W. Gadzuk and M. Šunjić, *Phys. Rev. B* **12**, 524 (1975).
- <sup>48</sup>D. C. Langreth, *Phys. Rev. B* **1**, 471 (1970); D. C. Langreth, *Proceedings of Lectures given at the International Center for Theoretical Physics, Trieste* (IAEA, Vienna, 1977).
- <sup>49</sup>Evidence of dynamical relaxation on Auger spectra of metals has been recently given by: F. J. Himpsel, D. E. Eastman, and E. E. Koch, *Phys. Rev. Lett.* **44**, 214 (1980); J. C. Fuggle, R. Lässer, O. Gunnarson, and K. Schönhammer, *Phys. Rev. Lett.* **44**, 1090 (1980).
- <sup>50</sup>P. Ascarelli, *Solid State Commun.* **21**, 205 (1977).
- <sup>51</sup>F. Antonangeli, A. Balzarotti, A. Bianconi, P. Perfetti, P. Ascarelli, and N. Nisticò, *Solid State Commun.* **21**, 201 (1977).

- <sup>52</sup>C. Kunz, *J. Phys. (Paris)* **39** C-4, 112 (1978), and references therein. See also F. Bassani, *Appl. Opt.* **19**, 4093 (1980).
- <sup>53</sup>Core exciton spectra of metals have been recently considered by C. A. Swarts, J. D. Dow, and C. P. Flynn, *Phys. Rev. Lett.* **43**, 158 (1979).
- <sup>54</sup>T. A. Callcott, E. T. Arakawa, and D. L. Ederer, *Phys. Rev. B* **16**, 5185 (1977).
- <sup>55</sup>U. Von Barth and G. Grossmann, *Phys. Scr.* **21**, 580 (1980).
- <sup>56</sup>H. Hedin, in *X-ray Spectroscopy*, edited by L. V. Azaroff (McGraw-Hill, New York, 1974), p. 221.
- <sup>57</sup>I. M. Curelaru and G. Wendin, *Phys. Scr.* **22**, 513 (1980); I. M. Curelaru, E. Suoninen, and E. Minni, in *Inner-Shell and X-ray Physics of Atoms and Solids*, edited by D. J. Fabian, H. Kleinpoppen, and L. M. Watson (Plenum, New York, 1981), p. 593; *J. Chem. Phys.* (in press).
- <sup>58</sup>N. D. Lang and A. R. Williams, *Phys. Rev. B* **16**, 2408 (1977); *Phys. Rev. Lett.* **40**, 954 (1978).
- <sup>59</sup>A. Kotani and Y. Toyozawa, *J. Phys. Soc. Jpn.* **35**, 1073 (1973); **37**, 912 (1974).
- <sup>60</sup>A. Kotani, *Jpn. J. Appl. Phys. Suppl.* **17**, 212 (1978).
- <sup>61</sup>D. A. Goodings and R. Harris, *J. Phys. C* **2**, 1808 (1969).
- <sup>62</sup>D. A. Shirley, R. L. Martin, S. P. Kowalczyk, F. R. McFeely, and L. Ley, *Phys. Rev. B* **15**, 544 (1977).
- <sup>63</sup>C. M. K. Watts, *J. Phys. F* **2**, 574 (1972). If plasmon losses are neglected in Eq. (5),  $\rho_c(E - E') = \delta(E - E')$  and we recover the usual self-convolution of the valence-band DOS.
- <sup>64</sup>Values of the plasmon relaxation time ranging from 0.8 to  $1.1 \times 10^{-15}$  sec (0.8–0.6 eV) have been reported for the screened plasmon mode of TiN at 2.8 eV (Ref. 23). We have taken  $\gamma_p = 0.6$  eV for TiC since the relaxation time quoted in Ref. 9,  $\tau_p = 9.31 \times 10^{-15}$  sec, is too long compared to the Auger decay time for an effective coupling to the conduction electrons.
- <sup>65</sup>D. A. Papaconstantopoulos, *Phys. Rev. Lett.* **31**, 1050 (1973).
- <sup>66</sup>P. Rabe, *Jpn. J. Appl. Phys.* **17**, 23 (1978).
- <sup>67</sup>E. A. Stern, D. E. Sayers, and F. W. Lytle, *Phys. Rev. B* **11**, 4836 (1975).
- <sup>68</sup>J. J. Rehr, E. A. Stern, R. L. Martin, and E. R. Davidson, *Phys. Rev. B* **17**, 560 (1978).
- <sup>69</sup>R. Haensel, P. Rabe, G. Tolkhiehn, and A. Werner, in *Proceedings of Nato Advanced Study Institute, Liquid and Amorphous Metals*, edited by E. Lüscher (Reidel, Dordrecht, 1981).
- <sup>70</sup>M. De Crescenzi, A. Balzarotti, F. Comin, L. Incoccia, S. Mobilio, and N. Motta, *Solid State Commun.* **37**, 921 (1981).
- <sup>71</sup>P. Eisenberger and G. S. Brown, *Solid State Commun.* **29**, 481 (1979).
- <sup>72</sup>Yu. A. Babanov, V. V. Vasin, A. L. Ageev, and N. V. Ershov, *Phys. Status Solidi B* **105**, 747 (1981).
- <sup>73</sup>G. Martens, P. Rabe, N. Schwentner, and A. Werner, *Phys. Rev. B* **17**, 1481 (1978).
- <sup>74</sup>W. B. Pearson, *Handbook of Lattice Spacings and Structures of Metals and Alloys* (Pergamon, New York, 1958).
- <sup>75</sup>G. Beni and P. M. Platzmann, *Phys. Rev. B* **14**, 1514 (1976).
- <sup>76</sup>T. A. Carlson, *Photoelectron and Auger Spectroscopy* (Plenum, New York, 1975).
- <sup>77</sup>V. Moisy-Maurice, Centre d'Etude Nucléaires de Fontenay-aux-Roses, Commissariat à l'Energie Atomique (CEA) Report No. N2171 (unpublished).
- <sup>78</sup>G. Martens, P. Rabe, N. Schwentner and A. Werner, *Phys. Rev. Lett.* **39**, 1411 (1977).
- <sup>79</sup>A. Balzarotti, F. Comin, L. Incoccia, S. Mobilio, M. Piacentini, and A. Savoia, in *Inner-Shell and X-ray Physics of Atoms and Solids*, edited by D. J. Fabian, H. Kleinpoppen, and L. M. Watson (Plenum, New York, 1981), p. 723.